Optical spectroscopy and crystal-field analysis of $YAl_3(BO_3)_4$ single crystals doped with dysprosium

2003 J. Phys.: Condens. Matter 15 1047

(http://iopscience.iop.org/0953-8984/15/7/303)

INSTITUTE OF PHYSICS PUBLISHING JOURNAL OF PHYSICS: CONDENSED MATTER

J. Phys.: Condens. Matter **15** (2003) 1047–1056 PII: S0953-8984(03)55719-8

Optical spectroscopy and crystal-field analysis of $YAl_3(BO_3)_4$ single crystals doped with dysprosium

Enrico Cavalli[1,5], Enrico Bovero[1], Nicola Magnani[2], Mariola O Ramirez[3], Adolfo Speghini[4] and Marco Bettinelli[4]

[1] INFM and Dipartimento di Chimica GIAF, Università di Parma, Parco Area delle Scienze 17/A, I-43100 Parma, Italy
[2] INFM and Dipartimento di Fisica, Università di Parma, Parco Area delle Scienze 17/A, I-43100 Parma, Italy
[3] Departamento de Física de Materiales, C-IV, Universidad Autónoma de Madrid, Cantoblanco, E-28049, Madrid, Spain
[4] Dipartimento Scientifico e Tecnologico, Università di Verona and INSTM, UdR Verona, Ca' Vignal, Strada Le Grazie 15, I-37134 Verona, Italy

E-mail: enrico.cavalli@unipr.it

Received 7 November 2002
Published 10 February 2003
Online at stacks.iop.org/JPhysCM/15/1047

Abstract

$YAl_3(BO_3)_4$ crystals doped with Dy^{3+} were grown from a potassium trimolybdate flux. Their absorption and visible emission spectra and decay curves were measured at temperatures ranging from 10 to 298 K. The complete energy level scheme has been deduced from the low temperature measurements and reproduced by theoretical calculations based on a parametric Hamiltonian including coulombic, spin–orbit and crystal-field terms. The Judd–Ofelt parametrization scheme has been applied to the analysis of the room temperature absorption spectra. The calculated radiative lifetime of the $^4F_{9/2}$ state is 344 μs; this value is reasonably consistent with the experimental data.

1. Introduction

$YAl_3(BO_3)_4$ (YAB) is a huntite-type crystal with a non-centrosymmetric structure having interesting non-linear optical properties [1]. It has good physical properties and chemical stability, and the Y^{3+} ion can be easily replaced with other trivalent rare earth (RE) ions even at high concentrations to give optically active materials potentially suitable as active media in solid state laser devices. The optical properties of YAB doped with Nd^{3+} have been thoroughly investigated [2, 3], and it has been assessed that this is a promising material for diode pumped self-frequency doubling (SFD) lasers [4] as well as for red, blue and green laser generation [5]. Moreover, 1.1 W CW green output from a YAB:Yb laser has been recently obtained by Dekker *et al* [6], that is the highest green power reported to date for a diode pumped

[5] Author to whom any correspondence should be addressed.

SFD device. Much less information is available concerning YAB crystals activated with other RE ions, probably because they are not of consolidated technological interest, as is the case for Nd^{3+} and Yb^{3+} doped crystals. However, the prospective application of a laser medium can be reliably assessed only when its spectroscopic properties have been thoroughly investigated. For this reason we have grown a series of YAB crystals doped with different lanthanide ions and we are carrying out a systematic investigation of their optical spectra. Some preliminary results have been recently reported [7]. In this paper we present the results obtained in the case of crystals activated with Dy^{3+}. The interest in the optical properties of Dy^{3+} doped oxides is considerably increasing after the recent discovery of two novel visible laser channels in $KY(WO_4)_2$:Dy and $KGd(WO_4)_2$:Dy [8]. Moreover, Dy^{3+} doped garnets have been indicated as potential saturable absorbers in the 2.8 μm region [9]. In any case, whatever the application of the material, the knowledge of its optical spectroscopy is necessary. We have measured the 10 and 298 K absorption and emission spectra and the decay curves as a function of the temperature of YAB:Dy. The room temperature absorption spectra have been analysed in the frame of the Judd–Ofelt (JO) approach, and the intensity parameters have been evaluated from a least squares fit of the experimental oscillator strengths. These parameters have been used to calculate the spontaneous emission probabilities, the branching ratios and the radiative lifetime of the $^4F_{9/2}$ emitting level. This value has been compared with the results obtained from the measurement of the luminescence decay curves. The low temperature spectra have led to the determination of the energy level scheme of the Dy^{3+} ion in YAB. The electronic structure of the optically active ion has then been reliably reproduced by a quantum mechanical calculation based on a Hamiltonian including coulombic, spin–orbit and crystal-field (CF) terms.

2. Experimental details

2.1. Crystal growth and structure

The YAB:Dy crystals were grown by means of the 'flux growth' method [10], using $K_2Mo_3O_{10} + B_2O_3$ as a solvent in the 1200–700 °C temperature range. The dopant was added in suitable amounts as Dy_2O_3. Crystals with nominal 0.3, 2.8 and 5.8% Dy/Y molar ratios were grown and appropriately used for the spectroscopic measurements. YAB belongs to the trigonal system, space group $R32$ (huntite structure), with cell parameters $a = b = 9.295$ Å and $c = 7.243$ Å, $Z = 3$ [11]. The $Y^{3+}(Dy^{3+})$ sites have sixfold oxygen coordination and trigonal prismatic geometry with D_3 point symmetry. The Al^{3+} ions are in octahedral sites whereas the B^{3+} ones are surrounded by three oxygen atoms with triangular geometry. The $Y^{3+}(Dy^{3+})$ sites are well separated from one another (the Y^{3+}–Y^{3+} minimum distance is about 5.9 Å). This limits energy transfer and concentration quenching processes.

2.2. Spectroscopic measurements

The absorption and luminescence spectra and the decay curves were measured at temperatures ranging from 10 to 298 K. The absorption spectra were measured with a spectroscopic system equipped with a 300 W halogen lamp fitted with a 0.25 m Spex monochromator as source, and a 1.26 m Spex monochromator with an RCA C31034 photomultiplier, an EMI TE9684QB NIR extended photomultiplier or an NEP PbS cell to analyse and detect the output radiation. The luminescence spectra in the visible region (440–830 nm) were measured using the same set-up with the optical pathway properly modified and a 450 W xenon lamp replacing the halogen lamp. For the measurement of the luminescence decay curves, the sample was excited at 391 nm using the second harmonic of a Ti:sapphire pulsed laser pumped by a Nd:YAG

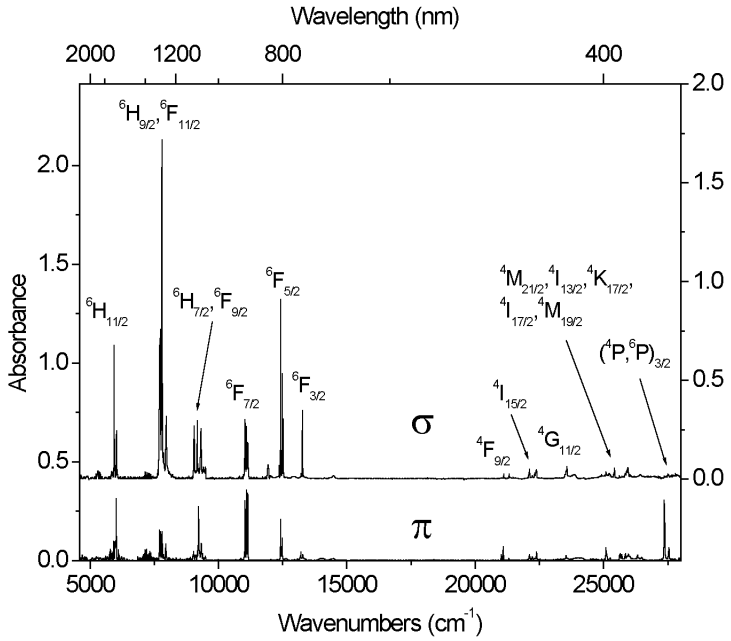

Figure 1. 10 K polarized absorption spectrum of YAB:Dy (5.8%). Crystal thickness: 1.23 mm.

laser (Quanta System); the emission was isolated by means of a Hilger–Watts model D330 double monochromator and detected with a Hamamatsu R943-022 photomultiplier connected to a LeCroy 9410 transient digitizer. The samples were cooled by means of an Air Products Displex DE 202 or a Galileo Vacuum Tech model K1 closed cycle cryostat.

3. Results and discussion

3.1. 10 K spectra and crystal-field analysis

The 10 K polarized absorption spectrum of YAB:Dy (5.8%) is reported in figure 1. It is composed of multiplets assigned to the transitions from the $^6H_{15/2}$ ground state to the excited levels arising from the $4f^9$ electronic configuration of Dy^{3+} [12]. They consist of sharp lines having FWHM (full width at half maximum) of the order of 10–20 cm^{-1}, whose number does not exceed that expected from the CF splitting of the involved levels. It can be noted that the most intense features lie in the NIR region of the σ spectrum. The 10 K luminescence spectrum presents four band systems assigned to the emissions from the $^4F_{9/2}$ excited state to the five lowest levels, as shown in figure 2, full curve. From these data we have been able to compile the energy level scheme of the Dy^{3+} in YAB, reported in table 1. The observed energy values have been reproduced using a Hamiltonian of the form

$$\hat{H} = \hat{H}_{FI} + \hat{H}_{CF} \tag{1}$$

where, according to [13], the free-ion part is written as

$$\hat{H}_{FI} = E_{av} + \sum_k F^k \hat{f}_k + \zeta \hat{H}_{S.O.} + \alpha L(L+1) + \beta \hat{G}(G_2) + \gamma \hat{G}(R_7) + \sum_i T^i \hat{t}_i + \sum_j M^j \hat{m}_j + \sum_k P^k \hat{p}_k \tag{2}$$

Table 1. Observed and calculated energy levels (cm^{-1}) for YAB:Dy.

$^{2S+1}L_J$	E_{exp}	E_{calc}	$^{2S+1}L_J$	E_{exp}	E_{calc}
	0	−5	$^4I_{15/2}$	22 104	22 107
	—	3		22 123	22 133
$^6H_{15/2}$	70	58		22 153	22 148
	227	229		22 232	22 266
	—	261		22 321	22 314
	322	322		22 391	22 393
	416	397		—	22 434
	458	436		—	22 467
	—	3 571	$^4G_{11/2}$	23 540	23 515
	3 580	3 574		23 584	23 597
	3 586	3 583		23 629	23 611
$^6H_{13/2}$	3 608	3 616		—	23 666
	3 658	3 688		—	23 683
	3 725	3 730		23 699	23 702
	3 778	3 769			
	5 860	5 849	$^4M_{21/2}$	24 863	
	—	5 931		24 925	
	5 961	5 956		25 050	
$^6H_{11/2}$	6 006	6 023		25 100	
	—	6 041		25 214	
	6 064	6 042		25 278	
				25 342	
				25 393	
				25 432	
	—	7 689	$^4I_{13/2} + {}^4K_{17/2}$	25 627	
	7 714	7697		25 680	
	7 731	7 721		25 720	
	7 756	7 764		25 759	
	7 777	7 807			
$^6H_{9/2} + {}^6F_{11/2}$	7 836	7 849			
	—	7 857			
	—	7 879			
	7 991	7 990			
	—	8 020			
	8 045	8 037			
	9 041	9 047	$^4I_{17/2}$	25 799	
	9 058	9 058		25 839	
	9 099	9 093		25 906	
$^6H_{7/2} + {}^6F_{9/2}$	9 182	9 193		25 947	
	—	9 196		26 041	
	9 242	9 217		26 096	
	9 328	9 349			
	9 337	9 351			
	9 389	9 367			
$^6H_{5/2}$	—	10 207	$^4M_{19/2}$	26 343	
	10 288	10 283		26 399	
	10 373	10 401		26 427	
				26 455	
				26 511	
				26 567	

Table 1. (Continued.)

$^{2S+1}L_J$	$E_{exp.}$	$E_{calc.}$	$^{2S+1}L_J$	$E_{exp.}$	$E_{calc.}$
	11 047	11 067	$(^4P, ^6P)_{3/2}$	27 367	
$^6F_{7/2}$	—	11 095		27 548	
	11 101	11 099			
	11 150	11 140			
	12 434	12 440	$^4I_{11/2}$	27 948	
$^6F_{5/2}$	12 493	12 497		28 026	
	12 534	12 507		28 074	
$^6F_{3/2}$	13 276	13 274	$^4M_{5/2} + {}^6P_{7/2}$	28 392	
	13 290	13 280		28 409	
$^6F_{1/2}$	—	13 818		28 441	
				28 506	
				28 522	
	—	20 958			
	21 026	21 039			
$^4F_{9/2}$	21 097	21 086			
	—	21 238			
	21 249	21 242			

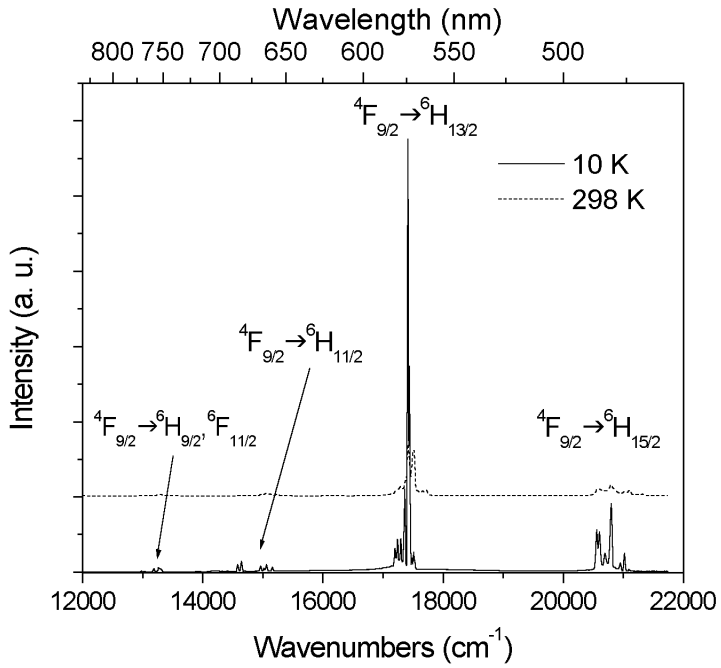

Figure 2. 10 and 298 K unpolarized emission spectrum of YAB:Dy (2.8%).

where $k = 2, 4, 6$; $i = 2, 3, 4, 6, 7, 8$; $j = 0, 2, 4$ and the D_3 CF Hamiltonian is written as

$$\hat{H}_{CF} = \sum_k \sum_q B_k^q \hat{C}_k^q = B_2^0\hat{C}_2^0 + B_4^0\hat{C}_4^0 + B_4^3(\hat{C}_4^{-3} - \hat{C}_4^3) + B_6^0\hat{C}_6^0 + B_6^3(\hat{C}_6^{-3} - \hat{C}_6^3) + B_6^6(\hat{C}_6^6 + \hat{C}_6^{-6}). \quad (3)$$

Table 2. Free-ion and CF parameters for Dy^{3+} in YAB.

Parameter	Value (cm^{-1})	Parameter	Value (cm^{-1})	Parameter	Value (cm^{-1})
E_{av}	56 238	T^2	329	P^2	719
F^2	91 891	T^3	36	P^4	359
F^4	63 077	T^4	127	P^6	72
F^6	50 032	T^6	−314	B_2^0	397
α	18 020	T^7	404	B_4^0	−1144
β	−633	T^8	315	B_4^3	−1094
γ	1 790	M^0	3.39	B_6^0	394
ζ	1 902	M^2	1.90	B_6^3	−18
		M^4	1.05	B_6^6	−378
				σ	14

This model Hamiltonian accounts for two-body electrostatic repulsion (F^k), two- and three-body configuration interactions (α, β, γ and T^i, respectively), spin–orbit coupling (ζ), spin–other-orbit interactions (M^j), electrostatically correlated spin–orbit interactions (P^k) and CF potential. A detailed description of the various free-ion operators and parameters is available in the literature [14]; the tensor operators $\hat{C}_k^q$ are defined in [15].

The single-ion parameters for Dy^{3+} in YAB were determined by fitting all the observed experimental levels lying below 24 000 cm^{-1}, using the procedure described in [13]. The levels lying above this energy value were not included in the calculation because the number of the components detected for every multiplet was not sufficient for a significant fit. The spherically symmetric one-electron part of the Hamiltonian was substituted by the E_{av} parameter, which shifts the energy value of the whole $4f^9$ configuration. Since $\hat{H}_{FI}$ is expected to be largely independent of the host, the free-ion parameters for Dy^{3+}:LaF_3 [13] were used as starting values, and only four of them (F^2, F^4, F^6 and ζ) were allowed to vary during the fitting procedure. Starting values for the CF parameters were determined both as point charge lattice sums using the procedure described in [16] and by means of the Newman superposition model (SPM) [17], considering only the contribution of the first coordination sphere around the Dy^{3+} ion. This coordination sphere is composed of six equivalent O^{2-} ligands, all at the same distance R_ℓ from the Dy^{3+} site; therefore, the ratios between CF parameters B_k^q with the same value of k calculated by the SPM is fixed and independent of the SPM parameters $\bar{B}_k(R_\ell)$ and t_k [17]. It has been found that the SPM ratios are more reliable than the lattice-sum ones; the former are consistent with those obtained from the best-fit procedure which concerns sign and magnitude, whereas some of the parameters calculated by the latter method (B_6^3 and B_6^6 in particular) strongly differ from the corresponding ones in the best-fit set. Thus, as regards the fourth- and sixth-order CF parameters, it may be inferred that the contributions of the next nearest neighbours to $\hat{H}_{CF}$ are almost negligible with respect to the CF potential due to the oxygen ligand cage. Non-negligible effects of the second coordination sphere on the second-order parameter B_2^0 are envisaged; however, a satisfying quantitative analysis is not possible since only one second-order non-zero parameter (B_2^0) is present in this system. The best fit of the experimental data has been carried out using the parameters reported in table 2. The resulting σ root mean square (rms) value, about 14 cm^{-1}, confirms the reliability of the fit. The experimental and the calculated energy level values are compared in table 1. Reasonable estimates of the fourth- and sixth-order SPM parameters for the Dy^{3+}–O^{2-} pair in YAB are $\bar{B}_4(R_\ell) = (760 \pm 40)$ cm^{-1} and $\bar{B}_6(R_\ell) = (250 \pm 80)$ cm^{-1}.

Table 3. Experimental and calculated oscillator strengths (P) of Dy^{3+} in YAB. The JO parameters, Ω_λ, the rms and the percentage error are also tabulated. $\Omega_2 = 1.59 \times 10^{-19}$ cm^2, $\Omega_4 = 9.51 \times 10^{-20}$ cm^2, $\Omega_6 = 2.58 \times 10^{-20}$ cm^2, rms $= 6.62 \times 10^{-7}$ (14.1%).

Excited state	Barycentre (cm^{-1})	P_{exp} (10^6)	P_{calc}(10^6)
$^6H_{11/2}$	5 948	1.64	2.26
$^6H_{9/2} + {}^6F_{11/2}$	7 748	20.4	20.4
$^6H_{7/2} + {}^6F_{9/2}$	9 027	7.10	7.33
$^6F_{7/2}$	11 011	4.60	3.78
$^6F_{5/2}$	12 453	2.18	1.21
$^6F_{3/2}$	13 267	0.55	0.23
$^4F_{9/2}$	21 201	0.26	0.28
$^4I_{15/2}$	22 243	0.91	0.70

As regards the lowest J multiplet ($^6H_{15/2}$), it is split by the CF into eight Kramers doublets and its total observed splitting is 458 cm^{-1}, whereas its total calculated splitting is 441 cm^{-1}. It is interesting to note that our CF calculations predict the presence of an energy level very close to the ground state ($\Delta E \approx 8$ cm^{-1}). This pseudo-quartet ground state cannot be confirmed or disproved by the optical spectra presented here, but may be verified by other experimental techniques.

3.2. 298 K spectra and Judd–Ofelt analysis

The components of the room temperature absorption and emission manifolds of YAB:Dy^{3+} are broader and less intense than those observed in the 10 K spectra. Some weak hot bands are also present, due to transitions originating from thermally populated Stark levels. The 298 K emission spectrum is shown in figure 2 (dotted curve); the corresponding absorption spectrum is not shown for the sake of brevity. The oscillator strengths of the absorption transitions have been carefully determined and fitted on the basis of the JO parametrization scheme [18, 19] after subtraction of the magnetic dipole contribution for the $^4I_{15/2} \leftarrow {}^6H_{15/2}$ transition. This contribution is small and not reported here. The reduced matrix elements were taken from Kaminskii [12], and the value of the refractive index was assumed to be $n = 1.74$, according to Filimonov *et al* [20]. The evaluated intensity parameters are reported in table 3, together with the observed and calculated oscillator strengths and the rms deviation. The calculated spontaneous emission probabilities and the radiative branching ratios for the transitions from the $^4F_{9/2}$ state to the lower ones are reported in table 4, together with the radiative lifetime of the emitting level. They were estimated using the calculated intensity parameters and the reduced matrix elements reported by Kaminskii [12]. The values of the branching ratios are in qualitative agreement with the relative intensities of the bands observed in the 298 K emission spectrum where the most intense manifold by far is that assigned to the $^4F_{9/2} \rightarrow {}^6H_{13/2}$ transition, located in the yellow region (575 nm). This could be particularly attractive for laser applications since solid state devices operating in this spectral region have not yet been developed.

3.3. Fluorescence dynamics

We have also measured the room temperature decay curves of the $^4F_{9/2}$ level in 0.3, 2.8 and 5.8% Dy^{3+} doped YAB upon pulsed excitation at 391 nm. They are shown in figure 3. It is evident that only in the case of the most diluted crystal is the decay a single exponential, and that the deviation from the exponential behaviour increases with the dopant concentration. In

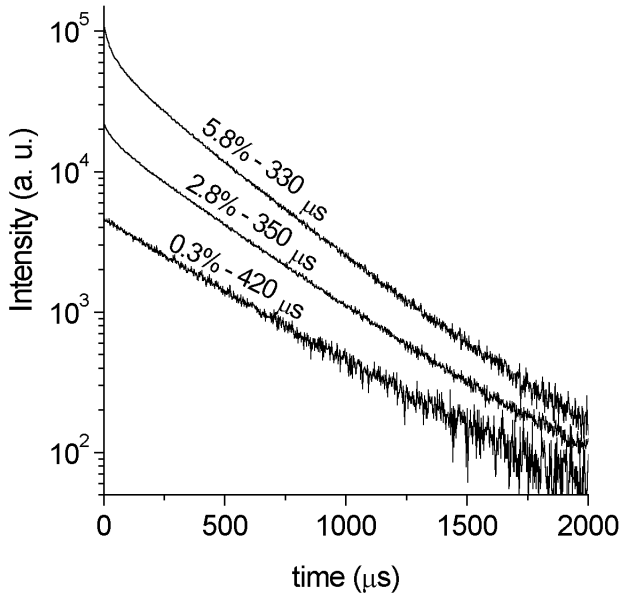

Figure 3. 298 K decay curves as a function of the dysprosium concentration.

Table 4. Calculated spontaneous emission probabilities A and radiative branching ratios β for the $^4F_{9/2}$ emitting level. Calculated radiative lifetime $\tau = 344$ μs.

Final state	A (s^{-1})	β
$^6F_{5/2}$	25	0.009
$^6F_{7/2}$	19	0.006
$^6H_{5/2}$	16	0.006
$^6H_{7/2}$	0	0.000
$^6F_{9/2}$	40	0.014
$^6F_{11/2}$	74	0.025
$^6H_{9/2}$	55	0.019
$^6H_{11/2}$	219	0.075
$^6H_{13/2}$	2073	0.713
$^6H_{15/2}$	387	0.133

the case of the more concentrated crystals, the decay times reported in the figure have been evaluated by considering the long time tails of the decay curves, where they yielded a good single-exponential fit. This points towards the presence of short range interactions between the active ions. The radiative lifetime calculated by means of the JO method is not far from the value observed for the 0.3% doped sample, even if the agreement is not fully satisfactory. Anyway, this allows us to conclude that multiphonon relaxation processes are inactive, as expected from the relatively large energy gap between the emitting and the next lower level (about 6200 cm^{-1}), that requires the participation of at least five phonons, the maximum phonon energy of the lattice being 1378 cm^{-1} [21]. In order to obtain more information on the excited state dynamics of the Dy^{3+} ion, the decay curves of the 2.8% doped crystal were measured as a function of the temperature and decay times were extracted from the long time exponential tail of the curves. It was observed that the decay times increase with the temperature from 240 μs at 10 K to about 350 μs at room temperature (see figure 4). This behaviour is similar

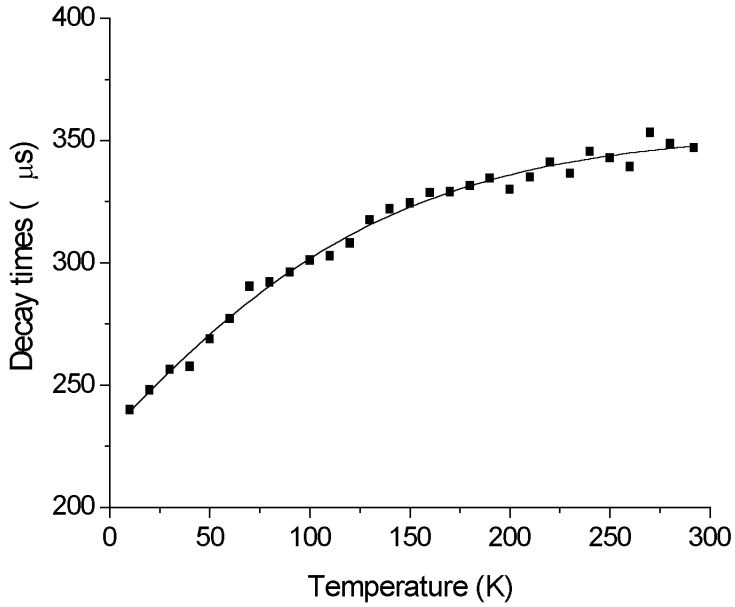

Figure 4. Temperature behaviour of the decay times of YAB:Dy (2.8%).

to that observed for Dy^{3+} in other hosts [21, 22] and has yet to be satisfactorily explained. Two kinds of mechanism can be reasonably considered. In the first one it is supposed that the probabilities of the radiative transitions of some upper Stark components of the $^4F_{9/2}$ multiplet are smaller than that of the lowest one. As the temperature increases, these components become populated and significantly contribute to the emission process, leading to an increase of the decay time. A similar behaviour has been observed in the case of Yb^{3+} ions in garnets [23]. The second possible mechanism is a cross relaxation process, among the various ones which can be supposed on the basis of the rich energy level scheme of the Dy^{3+} ion, where the resonance conditions are better fulfilled in the low temperature limit. In fact, with increasing temperature, line broadening effects can reduce the resonance and therefore decrease the efficiency of the process [24]. Experimental work is in progress in order to obtain more information on these mechanisms.

4. Concluding remarks

The electronic structure of the Dy^{3+} ion in YAB has been deduced from the 10 K absorption and emission spectra and reproduced by means of quantum mechanical calculations based on a Hamiltonian consisting of coulombic, spin–orbit and CF terms. A comparison between the best-fit and the theoretical values of the B_k^q parameters allowed us to infer that the CF potential at the RE site is essentially due to the six nearest neighbour oxygen ions: in fact the contribution of the ligands external to the first coordination sphere has been found to be smaller than that expected on the basis of the lattice-sum calculations. The JO theory has been applied to the analysis of the room temperature absorption spectra and the intensity parameters have been evaluated. They are consistent with those reported for Dy^{3+} in other hosts [22, 24]. The calculated lifetime is close to the measured value, indicating that multiphonon relaxation is inefficient. Nevertheless, the excited state dynamics of this material is still not fully understood,

in particular as concerns the temperature behaviour of the lifetimes, and the cross relaxation processes. As a final consideration, we point out that the emission spectrum of YAB:Dy is dominated by the $^4F_{9/2} \rightarrow {}^6H_{13/2}$ transition at 575 nm; this behaviour is of potential interest in order to develop new solid state lasers in the yellow region.

Acknowledgment

This work has been carried out with the financial support of the Ministero dell'Istruzione, dell'Università e della Ricerca (project COFIN 2001).

References

[1] Becker P 1998 *Adv. Mater.* **10** 979
[2] Jaque D, Muñoz J A, Cussó F and Garcia Solé J 1998 *J. Phys.: Condens. Matter* **10** 7901
[3] Jaque D, Capmany J, Luo Z D and Garcia Solé J 1998 *J. Opt. Soc. Am.* B **15** 6
[4] Hemmati H 1992 *IEEE J. Quantum Electron.* **28** 1169
[5] Jaque D, Capmany J and Garcia Solé J 1999 *Opt. Eng.* **38** 1794
[6] Dekker P, Davies J M, Piper J A, Liu Y and Wang J 2001 *Opt. Commun.* **195** 431
[7] Cavalli E, Speghini A, Bettinelli M, Ramírez M O, Romero J J, Bausá L and García Solé J 2003 *J. Lumin.* submitted
[8] Kaminskii A, Hömmerich U, Temple D, Seo J T, Ueda K, Bagayev S and Pavlyuk A 2000 *Japan. J. Appl. Phys.* **39** L208
[9] Seltzer M D, Wright A O, Morrison C A, Wortman D E, Gruber J B and Filer E D 1996 *J. Phys. Chem. Solids* **57** 1175
[10] Bartl M H, Gatterer K, Cavalli E, Speghini A and Bettinelli M 2001 *Spectrochim. Acta* A **57** 1981
[11] Belokoneva E L, Azizov A V, Leonyuk N I, Simonov M A and Belov N V 1981 *Zh. Strukt. Khim.* **22** 196
[12] Kaminskii A A 1996 *Crystalline Lasers: Physical Processes and Operating Schemes* (Boca Raton, FL: Chemical Rubber Company Press)
[13] Carnall W T, Goodman G L, Rajnak K and Rana R S 1989 *J. Chem Phys.* **90** 3443
[14] Crosswhite H M and Crosswhite H 1984 *J. Opt. Soc. Am.* B **1** 246 and references therein
[15] Wybourne B G 1965 *Spectroscopic Properties of Rare Earths* (New York: Interscience)
[16] Morrison C A and Leavitt R P 1979 *J. Chem. Phys.* **71** 2366
[17] Newman D J and Ng B 2000 *Crystal Field Handbook* (Cambridge: Cambridge University Press)
[18] Judd B R 1962 *Phys. Rev.* **127** 750
[19] Ofelt G S 1962 *J. Chem. Phys.* **37** 511
[20] Filimonov A A, Leonyuk N I, Meissner L B, Timchenho T I and Reiz I S 1974 *Kryst. Tech.* **9** 63
[21] Xia H R, Li L X, Wang J Y, Yu W T and Yang P 1999 *J. Raman Spectrosc.* **30** 557
[22] Cavalli E, Bovero E and Belletti A 2002 *J. Phys.: Condens. Matter* **14** 5221
[23] Bogomolova G A, Vylegzhanin D N and Kaminskii A A 1976 *Sov. Phys.–JETP* **42** 440
[24] Hanuza J, Macalik L, Ryba-Romanowski W, Mugenski E, Cywinski R, Witke K, Piltz W and Reich P 1988 *J. Solid State Chem.* **73** 488